Originally published in *Proceedings of the Fifth International Workshop on Compressible Turbulent Mixing*, ed. R. Young, J. Glimm & B. Boston. ISBN 9810229100, World Scientific (1996).

Single–Mode Rayleigh–Taylor Experiments in 2D and 3D*

B. A. Remington, M. M. Marinak, S. V. Weber,
K. S. Budil, O. L. Landen, S. W. Haan,
J. D. Kilkenny, and R. J. Wallace

Lawrence Livermore National Laboratory
Livermore, CA 94550

Abstract. Single-mode experiments have been conducted on the Nova laser to examine the effect of perturbation shape on ablation front Rayleigh-Taylor growth. The perturbations investigated had the same magnitude wave vector $k = (k_x^2 + k_y^2)^{1/2}$ and the same initial amplitude. The shapes corresponded to 2D $\lambda = 50$ μm, 3D square $k_x = k_y$, and stretched $k_x = 3k_y$ perturbations. We observed that the 3D perturbations grew more than the 2D perturbation. Numerical simulations in 2D and 3D are in agreement, showing the most symmetric modes growing the largest.

1 Introduction

Understanding the Rayleigh-Taylor (RT) instability is of critical importance to inertial confinement fusion (ICF) because large RT growth on imploding capsules can degrade implosion performance. In direct drive, non-uniformities in laser illumination imprint non-uniformities onto the capsule pusher ablation front. In indirect drive, residual capsule surface imperfections lead to perturbations at the ablation front. In both cases, the ablation front is RT unstable and perturbations grow. In the linear regime, the perturbation growth in the steady state is exponential,

$$\eta = \eta_o e^{\gamma t} \tag{1}$$

where η represents perturbation amplitude and the growth rate γ can be written approximately as [1, 2, 3]

$$\gamma = \left[\frac{\mathrm{kg}}{(1+\mathrm{kL})}\right]^{1/2} - \beta \mathrm{k} \mathrm{v_a}. \tag{2}$$

*We are pleased to acknowledge the assistance of S. G. Glendinning with software, invaluable discussions with D. Shvarts at the inception of this work, and the highly skilled Nova technical staff.

Here g is acceleration, $k = 2\pi/\lambda$ is perturbation wave vector, L is the density gradient scale length, β is a constant between 1 and 3, and v_a is ablation velocity. When the perturbation spatial amplitude is non-negligible compared to its wavelength, the RT evolution enters the nonlinear regime. For semi-infinite, incompressible fluids, the bubble approaches its terminal velocity, corresponding to the buoyancy being exactly balanced by kinematic drag [4, 5]. In this limit the bubble amplitude is just $\eta(t) = \int u_B dt$, with bubble velocity

$$u_B = a(gk)^{1/2} \tag{3}$$

where $a = 0.23$ in 2D and 0.36 in 3D, and we have assumed an Atwood number of 1 for simplicity. Notice that for the same perturbation wavelength (bubble diameter) λ, the bubble velocity is larger in 3D, since the kinematic drag per unit volume is less.

Perturbation growth is sensitive to perturbation shape. The transition to the nonlinear regime occurs approximately when the bubble velocity in the linear regime equals the nonlinear terminal bubble velocity, namely, when $\dot{\eta}_{\text{linear}} = \gamma\eta \approx u_B$. Since u_B is larger in 3D than in 2D from Eq. 3 the transition to the nonlinear regime happens later in 3D. Hence, in 3D the linear regime exponential growth phase lasts longer and the asymptotic nonlinear growth rate is higher. Single-mode perturbations therefore are expected to grow larger in 3D than the equivalent perturbation in 2D. This simple qualitative picture is supported by 3rd order perturbation theory [6], recent work with a potential flow model [5], and full numerical simulations [7, 8, 9]. Until recently, however, experiments in the ICF regime have been lacking due to their complexity. We present here new results of an experimental and computational investigation of 2D versus 3D single-mode perturbation growth at the ablation front in planar, indirectly driven foils [10]. Recent advances in target fabrication [11] and diagnostic development [12] have made this experiment possible.

The experimental configuration is shown in Fig. 1(a) and is described in more detail elsewhere [13]. A 750 μm diameter, 60 μm thick CH(Br) planar foil ($C_{50}H_{47}B_3$, $\rho = 1.26$ g/cm^3) is mounted across a diagnostic hole on a 3 mm long, 1.6 mm diameter gold cylindrical Hohlraum. Eight of the 10 Nova laser beams [14] are used to generate a 3.3 ns low-adiabat, shaped drive, as shown in Fig. 1(b). Two 3 ns square beams are delayed relative to the drive and focused onto a Sc backlighter disk to generate 4.3 keV He-α x-rays to back-illuminate the accelerating planar foil. Random phase plates with 5 mm diameter hexagonal elements are inserted as the last optic in the two backlighter lasers to generate a smooth 700 μm diameter x-ray spot. Typical timing of the backlighter lasers relative to the drive lasers is illustrated in Fig. 1(b). On each laser shot, two-dimensional gated x-ray images were obtained with a new flexible gated x-ray pinhole camera [12]. Four pinhole images are obtained for each strip on the MCP, and the inter-strip delay was set to 700 ps. The pinholes were filtered with 12.5 μm of Ti to eliminate higher energy backlighter x-rays such as from He-β and He-γ transitions in

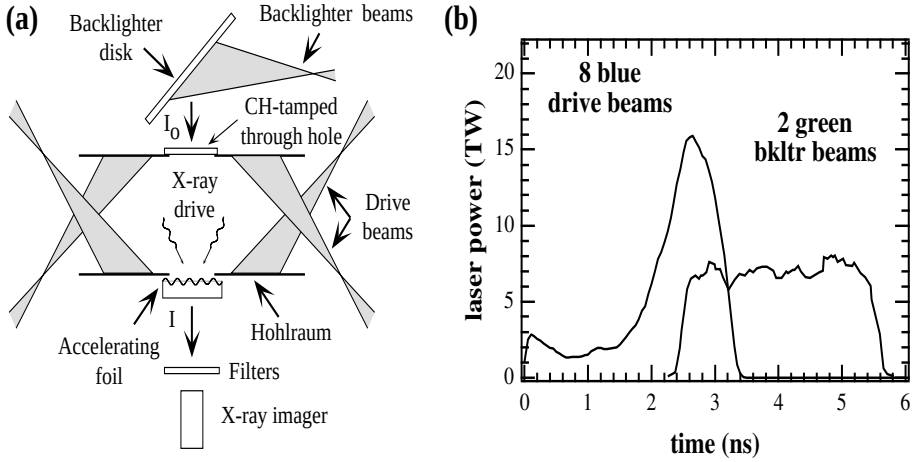

Figure 1: (a) The experimental configuration consists of a Au cylindrical Hohlraum with the modulated CH(Br) foil mounted on the wall. The laser beams convert to x rays in the Hohlraum, which ablatively accelerate the foil. Two additional laser beams generate backlighter x rays used for in-flight diagnosis of the foil. (b) Power versus time of one of the eight 0.351 μm wavelength drive laser beams (curves starting at t = 0) and one of the two 0.528 μm wavelength backlighter beams (curves starting at t = 2.4 ns).

Sc.

The foils were made using a new laser ablation technique to make molds in substrates of either kapton or mylar [11]. We prepared perturbed foils all with the same magnitude wave vector $k = (k_x^2+k_y^2)^{1/2}$ and nominally the same amplitude. The "2D" foil (1D wave vector $k = k_x$) was a simple $\lambda = 50$ μm sinusoid with initial amplitude $\eta_o = 2.5$ μm. One of the "3D" foils [2D wave vector $k = (k_x, k_y)$] corresponded to a "stretched" $k_x = 3k_y$ perturbation, and the other was a square $k_x = k_y$ mode. Characterization of the three foils was done using a contact radiography system, the resulting images of which are shown in Fig. 2(a-c), and contact profilometry. The radiographs were converted to spatial amplitudes using a step wedge of the same material, CH(Br). Images from the Nova shots at 4.3 ns, which is near peak growth, are shown in Fig. 2(d-f). The gated x-ray pinhole camera for these images was run at 8x magnification with 10 μm pinholes, and 150 μm Be filtering. The backlighter was scandium at 4.3 keV.

Each image from the Nova shots is converted to ln(exposure) $\propto -\mathrm{OD} = -\int \rho\kappa dz$. Hence, modulations in ln(exposure) correspond to modulations in foil areal density. The images are Fourier analyzed, and the amplitudes corresponding to the fundamental mode are extracted. For a purely experimental demonstration of the effects of dimensionality on perturbation growth, we did three shots where the only change made

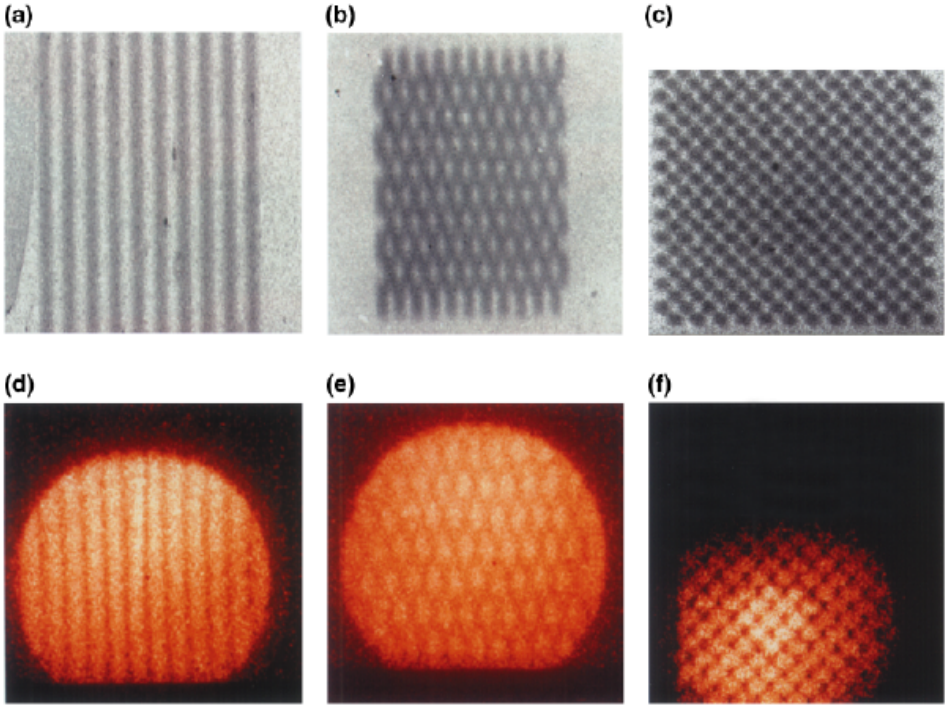

Figure 2: Contact radiographs of foils identical to those used in the Nova experiments are shown in (a)-(c). The perturbations correspond to (a) 2D $\lambda = 50$ μm, $\eta_o = 2.5$ μm, (b) 3D $k_x = 3k_y, \lambda_x = 53$ μm, $\lambda_y = 158$ μm, $\eta_o = 2.4$ μm, and (c) 3D $k_x = k_y, \lambda_x = \lambda_y = 71$ μm, $\eta_o = 2.7$ μm. The corresponding images from the Nova shots taken at 4.3 ns are shown in (d)-(f).

between shots was the target (2D $\lambda = 50$ μm versus 3D $k_x = k_y$ and $k_x = 3k_y$). The total laser energy for these shots was similar, and the timing and filtering of the diagnostic were identical. The results for the evolution of the fundamental mode is shown in Fig. 3(a). The $k_x = k_y$ square 3D mode grows the largest, the $\lambda = 50$ μm 2D mode grows the least, and the $k_x = 3k_y$ stretched 3D mode falls in between.

Shape effects on perturbation evolution can be examined under identical conditions with computer simulations. This is shown in Fig. 3(b) using the new 3D radiation-hydrodynamics code HYDRA [10]. The perturbations, in order of decreasing peak growth, correspond to $k_x = k_y, k_x = 2k_y, k_x = 3k_y$, and 2D $\lambda = 50$ μm. Our simulations clearly show that the most symmetric perturbations grow the largest, as has been reported by others [6, 7, 8]. This is qualitatively in agreement with our experimental observations; quantitative comparisons are currently underway.

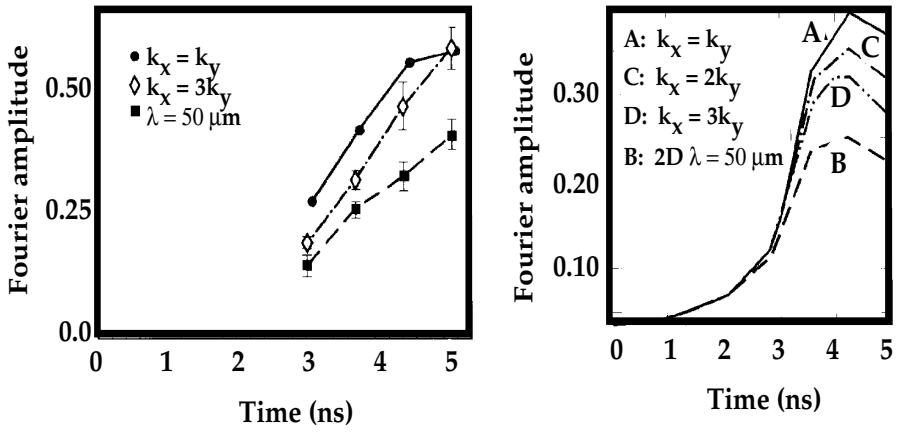

Figure 3: (a) Results of the evolution of the fundamental mode Fourier amplitude of ln(exposure) for the 3D $k_x = k_y$ (solid circles), $k_x = 3k_y$ (open diamonds), and 2D $\lambda = 50$ μm (solid squares) perturbations. The connecting lines are meant only to guide the eye. Experimental conditions were kept the same for theses shots to best illustrate the effect of shape on perturbation growth. The diagnostic setup was the same as described in Fig. [1]. (b) Predicted Fourier amplitude of ln(exposure) from 3D simulations for the evolution of four different perturbation shapes all with the same magnitude $k = (k_x^2 + k_y^2)^{1/2}$ wave vector, for drive conditions slightly different from those of (a). The most symmetric ($k_x = k_y$) mode is predicted to grow the largest, the 2D $\lambda = 50$ μm mode grows the least, and the 3D stretched cases fall in between, in agreement with the experiments.

References

[1] H. Takabe *et al.*, *Phys. Fluids* **26**, 2299 (1983); *ibid* **28**, 3676 (1985).

[2] D.H. Munro, *Phys. Rev. A* **38**, 1433 (1988).

[3] M. Tabak *et al.*, *Phys. Fluids B* **2**, 1007 (1990).

[4] D. Layzer, *Astrophys. J.* **122**, 1 (1955).

[5] U. Alon *et al.*, *Phys. Rev. Lett.* **72**, 2867 (1994); *ibid* **74**, 534 (1995).

[6] J.W. Jacobs and I. Catton, *J. Fluid Mech.* **187**, 329 (1988).

[7] J.P. Dahlburg *et al.*, *Phys. Fluids B* **5**, 571 (1993).

[8] J. Hecht *et al.*, *Phys. Fluids* **6**, 12 (1994);*Lasers and Part. Beams* **13**, 423 (1995).

[9] D. Youngs, *Lasers and Part. Beams* **12**, 725 (1994).

[10] M.M. Marinak *et al.*, *Phys. Rev. Lett.* **75**, 3677 (1995) and *Phys. Plasmas*, in press (1996).

[11] R.J. Wallace *et al.*, *ICF Quarterly Report* **4**, 79 (1994).

[12] K.S. Budil *et al.*, in press *Rev. Sci. Instrum.* (1996).

[13] B.A. Remington *et al.*, *Phys. Plasmas* **2**, 241 (1995).

[14] J.D. Kilkenny *et al.*, *Rev. Sci. Instrum.* **63**, 4688 (1992).